Journal of Materials Chemistry A

# In-Situ Formation of Zeolitic-Imidazolate Framework Thin Films and Composites Using Modified Polymer Substrates



| | |
|---|---|
| Journal: | *Journal of Materials Chemistry A* |
| Manuscript ID | TA-ART-01-2019-000837.R1 |
| Article Type: | Paper |
| Date Submitted by the Author: | 11-Mar-2019 |





| | |
|---|---|
| Complete List of Authors: | Abdul Hamid, Mohamad Rezi; Texas A and M University System, Chemical Engineering<br>Kim, Sunghwan; Texas A&M University at College Station, Chemical Engineering<br>Kim, Ju Sung; Hanyang University, College of Engineering, School of Chemical Engineering<br>Lee, Young Moo; Hanyang University, College of Engineering, School of Chemical Engineering; Hanyang University, College of Engineering, WCU Department of Energy Engineering<br>Jeong, Hae-Kwon; Texas A&M University at College Station, Chemical Engineering |

Journal of Materials Chemistry A

ARTICLE

# *In-Situ* Formation of Zeolitic-Imidazolate Framework Thin Films and Composites Using Modified Polymer Substrates

Received 00th January 20xx,
Accepted 00th January 20xx

DOI: 10.1039/x0xx00000x

www.rsc.org/

Mohamad Rezi Abdul Hamid,[a] Sunghwan Park,[a] Ju Sung Kim,[c] Young Moo Lee[c] and Hae-Kwon Jeong*[a,b]

It is of great interest to form polycrystalline metal-organic framework (MOF) thin films on polymer substrates or MOF/polymer composites for their practical applications in sensing and separations. It is, however, quite challenging to fabricate high-quality MOF thin films on polymer substrates or MOF/polymer composites in a facile manner. Herein, we report a simple *in-situ* method to fabricate high-quality zeolitic-imidazolate framework ZIF-8 thin films supported on polymers as well as ZIF-8/polymer composites by doping polymers with zinc ions followed by solvothermal treatment in a linker solution. Effects of key synthesis parameters on the microstructures of ZIF-8 thin films and composites were systematically studied. Formation of ZIF-8 crystals was confirmed using ATR-FTIR, EDX, XRD, SEM, and TEM. While continuous ZIF-8 films were observed on the substrate surfaces, it was revealed that ZIF-8 particles formed inside the substrates as well (i.e., ZIF-8/polymer mixed-matrix layers). The thicknesses of the mixed-matrix layers were demonstrated controllable by varying the kinetics of alkali hydrolysis. The method was applied to a family of ZIFs (i.e., ZIF-8 and ZIF-67) and mixed-metal ZIF-8 analogues, proving its versatility. Finally ultra-thin well-intergrown ZIF-8 membranes were prepared by secondarily growing ZIF-8 films on Matrimid® hollow fibers, showing promising propylene/propane separation performances.

## 1. Introduction

Metal-organic frameworks (MOFs) with unique properties have drawn considerable attention for a variety of advanced applications including gas storage,[1] separation,[2] sensing,[3] and catalysis.[4] Zeolitic-imidazolate frameworks (ZIFs),[5, 6] a subclass of MOFs, are one of the most widely studied MOFs on account for their ultramicroporosities (< 5.0 Å) and chemical/thermal stabilities relative to other MOFs. ZIFs are typically constructed by linking divalent metal ions (e.g., $Zn^{2+}$ and $Co^{2+}$) with imidazolate-based linkers forming open structures analogous to those of zeolites. While MOF materials are readily applicable in bulk/powder forms as adsorbents and catalysts,[7, 8] advanced applications including film-based sensors and separation membranes require them to be fabricated as thin films typically supported on substrates[9, 10] or composites with other materials.[11-13]

To date, MOF thin films have been predominantly grown on inorganic ceramic supports especially for membrane applications.[14-17] Ceramic supports are, however, relatively expensive, thereby increasing the cost of MOF thin films/membranes. In contrast, polymer substrates are cheap, scalable, and prevalent in commercial market, thereby more attractive for MOF thin films and composites. Nevertheless, there are only a limited number of reports on the synthesis of MOF thin films on either dense or porous polymer substrates. Typical synthesis methods to form MOF thin films include *in-situ*,[18-20] secondary (i.e., seeded) growth,[21-24] layer-by-layer,[25] and interfacial growth.[26, 27] Centrone et al.[28] were the first to report MOF thin films on polymer supports under microwave irradiation. They found that conversion of the nitrile groups of the polyacrylonitrile substrates to carboxylic acid groups was a requisite for the nucleation and growth of MIL-47 crystals on the substrates. Wang and co-workers[29] reported synthesis of ZIF-8 thin films on porous nylon substrates using counter-diffusion method. Nagaraju et al.[30] have demonstrated the formation of Cu-BTC and ZIF-8 thin films on porous asymmetric ultrafiltration polymer membranes using *in-situ* crystallization, followed by layer-by-layer deposition to form continuous MOF layers. Nair et al.[31] reported synthesis of ZIF-8 membranes on Torlon® hollow fibers using the interfacial microfluidic membrane processing technique where two immiscible solvents (octanol-water) interfacial approach can be precisely controlled to achieve a positional control over membrane formation. To enhance the heterogeneous nucleation of MOFs on polymer substrates, intermediate coating layers such as ATPES ((3-aminopropyl)triethoxysilane)-functionalized $TiO_2$[32] or Zn-based sol[33] were often utilized, resulting in ultra-thin ZIF-8 membranes. Although these reports demonstrate successful preparation of MOF thin films on polymer substrates, multiple

[a] Artie McFerrin Department of Chemical Engineering, Texas A&M University, College Station, TX 77843-3122, USA. E-mail: hjeong7@tamu.edu
[b] Department of Materials Science and Engineering, Texas A&M University, College Station, Texas 77843-3122, USA.
[c] Department of Energy Engineering, College of Engineering, Hanyang University, Seoul 133-791, Republic of Korea.
† Electronic Supplementary Information (ESI) available. See DOI: 10.1039/x0xx00000x

synthesis steps (e.g., repeated growth cycles, substrate functionalization, intermediate coating layers, etc.) add a degree of complexity, thereby increase the cost of resulting films. In addition, most of the literatures report synthesis of MOF/ZIF thin films on polymer flat sheets that have relatively low packing density. With a few exceptions,[26, 31, 34, 35] deposition of MOF/ZIF thin films were typically performed on and limited to easily accessible external surfaces. For practical separation applications, it is critical to synthesize MOF/ZIF thin films on substrates with high-surface-to-volume ratio (i.e., hollow fiber) to provide high packing density. In addition, MOF/ZIF thin films grown on the inner surface (bore side) of hollow fibers have advantage where these fibers can be bundled together in close proximity without compromising the relatively fragile MOF/ZIF layer, to form membrane module with high packing density. However, synthesizing MOF/ZIF thin films/membranes in a confined space (i.e., bore side) of the hollow fibers is more challenging than growing on the easily accessible external surface (i.e., shell side), as evidenced by the very limited number of scientific works available in literature.

Recently, Tsuruoka et al.[36] reported a general methodology for the formation of Al-based MOF (MIL-53(Al) = $[Al(OH)(bdc)]_n$, bdc = 1,4-benzenedicarboxylate) films on pyromellitic dianhydrides oxidianiline (PMDA-ODA, trademarked as Kapton®) polymer substrates based on an interfacial reaction approach using metal-doped polymers as substrates under microwaves. A PMDA-ODA polyimide film was first hydrolyzed in an alkali KOH solution, resulting in a potassium polyamate salt containing potassium carboxylate groups. Potassium cations were then ion-exchanged with aluminum cations. Subsequent microwave-heating of the $Al^{3+}$-exchanged polyamate salt in a 1,4-benzenedicarboxylic acid linker solution led to the interfacial self-assembly of MIL-53 crystals on the modified polymer substrate. Thickness and crystal density of the resulting MOF thin film were readily controlled by manipulating alkali treatment time and $Al^{3+}$ elution rate, respectively. In their later works,[37, 38] they were able to control the morphology and anisotropic growth of Cu-based MOF (Cu-based MOF = $[Cu_2(ndc)_2(dabco)]_n$, ndc = 1,4-naphthalene dicarboxylate, dabco = 1,4-diazabicyclo[2.2.2]octane) thin films on PMDA-ODA substrates by controlling linker concentration in the synthesis solution. Although the interfacial growth approach is expected to be a versatile strategy for the construction of MOF films on polymer substrates, there are no reports on successful fabrication of ZIF thin films using a similar approach. Moreover, the current interfacial reaction approach by Tsuruoka and his co-workers[36] resulted only in MOF film formation on polymer surfaces (i.e., external surfaces). It is often desirable to form MOF crystals inside polymer substrates (i.e., mixed-matrix composite films) as the resulting composites offer new features and functionalities that can be applied for advanced applications such as mixed-matrix membranes.[13]

Herein, we report facile *in-situ* preparation of well-intergrown zeolitic-imidazolate framework ZIF thin films on polyimide surfaces as well as well-dispersed ZIF nanoparticles inside the polymers (i.e., ZIF/polymer composites) using a modified interfacial reaction approach. Instead of relying on combination of counter cations and high temperature condition (enabled by microwave heating) to liberate the strongly coordinated $Zn^{2+}$ ions with carboxylic groups in the modified polymer layer,[36] our method takes advantage of free $Zn^{2+}$ ions present in the polymer free volume, thereby enabling the formation of ZIF thin films and composites at a relatively lower temperature without using counter cation species in the linker solution. In addition, it is found that one can form ZIF-8 thin films on different polyimide substrates with various geometries including hollow fibers. In this work, we focus primarily on ZIF-8, ZIF-67 (Co-substituted ZIF-8), and Zn/Co mixed-metal ZIF-8 analogues which are of particular interest for gas separation applications. Using ZIF-8 thin films on Matrimid® hollow fibers as seed layers, well-intergrown ZIF-8 membranes were prepared by secondary growth and tested for propylene/propane separation.

## 2. Experimental

### 2.1 Methods

Kapton® films (pyromellitic dianhydrides oxidianiline (PMDA-ODA), 50 µm thick, DuPont) were purchased and used as received. Matrimid® 5218 powder was kindly provided by Huntsman Advanced Materials. Potassium hydroxide (KOH, reagent grade, VWR International) was used as a hydrolyzing agent. Zinc nitrate hexahydrate ($Zn(NO_3)_2{\cdot}6H_2O$, 98 %, Sigma-Aldrich), cobalt nitrate hexahydrate ($Co(NO_3)_2{\cdot}6H_2O$, 98 %, Sigma-Aldrich), and 2-methylimidazole ($C_4H_6N_2$, 99 %, Sigma-Aldrich, hereafter HmIm) were used as metal and linker sources, respectively. Sodium formate (HCOONa, 99 %, Sigma-Aldrich) was used as a deprotonating agent. Methanol ($CH_3OH$, > 99 %, Alfa-Aesar), ethanol ($C_2H_5OH$, 94 - 96 %, Alfa-Aesar), dimethylformamide ($C_3H_7NO$, > 99 %, Alfa-Aesar, hereafter DMF), tetrahydrofuran ($C_4H_8O$, > 99 %, Alfa-Aesar, hereafter THF), hexane ($C_6H_{14}$, ACS grade, VWR International), and deionized (DI) water were used as solvents. All chemicals were used as received without further purification.

### 2.2 Preparation of porous Matrimid® hollow fibers and flat sheets

Porous Matrimid® hollow fibers were fabricated by a dry-wet jet spinning process following a procedure previously optimized and reported.[39] Dope and bore solution compositions as well as spinning parameters were appropriately manipulated to obtain hollow fibers with porous morphology on both bore and shell side. Asymmetric Matrimid® flat sheet substrates were prepared by the dry-wet phase inversion method.[40] The polymer dope solutions were prepared by dissolving Matrimid® powder (1.25 g, 25.0 wt %) in THF (0.86 g, 17.2 wt %) and DMF (2.59 g, 51.8 wt %) co-solvent mixture. The co-solvent of the volatile THF and the non-volatile DMF with 1:3 ratio was used to increase the local polymer concentration at the surface during the drying step, forming asymmetric structures. A non-solvent, ethanol (0.30 g, 6.0 wt %) was added to the mixture to increase phase inversion rate. Mixing process was done at room temperature overnight. The dope solution was poured on a flat glass substrate and casted using a film casting knife with

clearance of 346 µm. The volatile components were evaporated for 15 s in air. Then, the as-casted films were immediately immersed in water at 25 °C for 24 hrs. The films were solvent exchanged in ethanol for 30 min and then in hexane for 30 min. Finally, the films were dried at room temperature in air for 1 hr and further dried at 60 °C for 2 hrs.

### 2.3 Surface modification and metal doping of polymer substrates

Modification and ion-exchange of Kapton® and Matrimid® films were performed following a procedure reported by Tsuruoka et al.[36] with a slight adjustment. Pristine Kapton® and Matrimid® films (2.5 × 2.5 $cm^2$) were treated in a 5 M aqueous KOH solution at 50 °C for different periods of time, and then rinsed with DI water. One sides of the films were sealed with epoxy to ensure that the surface modification took place only on the exposed sides. Next, the films were immersed in a 100 mM aqueous zinc nitrate hexahydrate solution for 1 hr. The films were then rinsed with DI water. Excess metal solution and DI water on the films were carefully removed using Kimwipes.

### 2.4 *In-situ* solvothermal formation of ZIF-8 crystals on and in polymer substrates

To form ZIF-8 crystals on and inside the polymer substrates, the $Zn^{2+}$-doped polymer films were solvothermally treated in a linker solution based on our previously reported recipe[16] with a minor modification. Briefly, a linker precursor solution was prepared by dissolving 2.59 g of HmIm and 0.125 g of sodium formate in 30 ml of methanol (hereafter, linker solution). A $Zn^{2+}$-doped polymer film was positioned vertically in a Teflon-lined autoclave containing the linker solution. The autoclave was kept in a convection oven at 120 °C for 2 hrs. The sample was then rinsed with methanol several times and washed with fresh methanol overnight.

### 2.5 Characterization

Powder X-ray diffraction patterns were collected using a Rigaku Miniflex II powder X-ray diffractometer with Cu-Kα radiation (λ = 1.5406 Å). Attenuated total reflection Fourier transform infrared spectra were obtained using a Thermo Nicolet iS5 with a diamond ATR sampling accessory, accumulating total of 16 scans from 400 to 4000 $cm^{-1}$ with a resolution of 0.241 $cm^{-1}$. X-ray photoelectron spectra were collected on an Omicron XPS system with a DAR 400 dual Mg/Al X-ray source. Scanning electron micrographs were obtained using a JEOL JSM-7500F operating at 5 keV acceleration voltage and 15 mm working distance. Energy dispersive X-ray spectroscopy line profile analysis was performed using an Oxford EDS system operated at 20 keV acceleration voltage and 8 mm working distance. Transmission electron micrographs were obtained using a FEI Tecnai F20 electron microscope equipped with a thermal (Schottky) field-emission gun. Electron transparent specimens were prepared prior to imaging. Briefly, the samples were embedded in an epoxy resin and allowed to cure for 24 hrs under heat. The resin block was then silver sectioned (i.e., 60 - 90 nm thick) using a Leica UC7 ultra-microtome. Then, the thin sections were collected and transferred directly on a 300 mesh copper grid. The gas separation properties of ZIF-8 membranes on hollow fibers were determined using the Wicke-Kallenbach technique (Fig. S1) carried out at room temperature (~ 20 °C) under atmospheric pressure. An equimolar propylene/propane mixture was supplied to feed (bore) side while argon sweeping gas was flowed to permeate (shell) side. Volumetric flow rates of both feed and sweep gases were set at 20 cc/min. The composition of the permeate stream was analyzed using a gas chromatography (Agilent GC 7890 A) equipped with a HP-PLOT/Q column.

## 3. Result and discussion

Fig. 1 presents a schematic illustration of the modified interfacial reaction process, what we refer to as the "polymer-modification-enabled *in-situ* metal-organic framework formation" (PMMOF) process. As shown in the illustration, the process starts with alkali-induced cleavage of the imide-rings of a pristine Kapton® polyimide (hereafter, KAP) or any polyimides, forming carboxylates which can serve as ion-exchangeable sites. It is noted that as illustrated in Fig. 1, only a part of the polyimide (typically less than 5 µm) was hydrolyzed. Immersion of the modified film into an aqueous metal solution (e.g., $Zn^{2+}$, $Co^{2+}$, etc.) initiates ion-exchange of $K^+$ ions with the metal ions of interest. It is noted that the formation of a polyamic acid potassium salt enhances the hydrophilicity of the film,[41] facilitating the diffusion of $Zn^{2+}$ into and inside the film. As depicted in Fig. 1, there are two different $Zn^{2+}$ ions: those relatively strongly coordinated with carboxyl groups as well as those free (i.e., unbound) in the hydrophilic free volume. Upon the *in-situ* solvothermal treatment of the $Zn^{2+}$-polyamate salt in

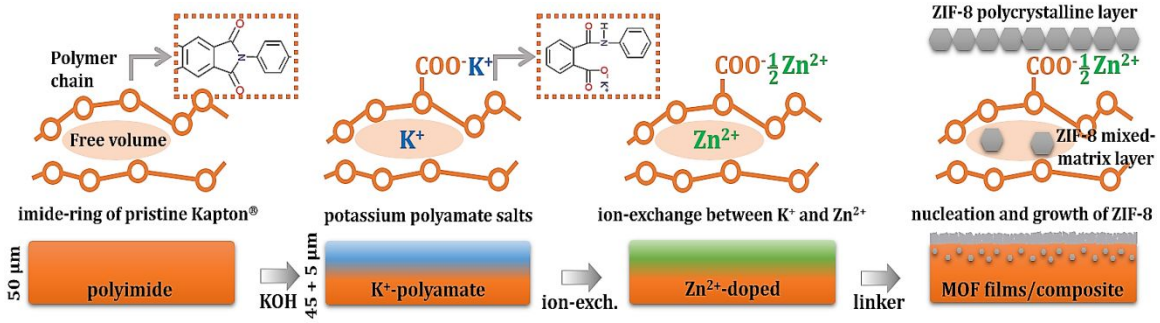


**Fig. 1.** Schematic illustration of the PMMOF approach enabling the solvothermal formation of ZIF-8 thin films on polymer substrates. It is noted that ZIF-8 crystals also form inside polymer substrates, depending on processing conditions

a HmIm linker solution, only free $Zn^{2+}$ ions elude from the free volume, resulting in the formation of continuous ZIF-8 layers on polymer surface as well as ZIF-8 crystals inside the polymer. The coordinated $Zn^{2+}$ ions on the other hand do not seem to participate in the formation of the crystals (will be discussed in later section). It is noted that even after extensive attempts, it was not possible to obtain ZIF-8 thin films using microwave heating as reported by Tsuruoka et al.[36] The PMMOF process is expected to be readily extended for the fabrication of MOF thin films on any polymer substrates, provided that the substrates are capable of undergoing similar chemistry.

Fig. 2a and S2 present the attenuated total reflection Fourier transform infrared (ATR-FTIR) spectra of pristine Kapton®, KOH-treated Kapton® (hereafter, KAP-x, x represents KOH treatment time in minutes), $Zn^{2+}$ ion-exchanged Kapton®, and ZIF-8 crystals grown on the polymer modified Kapton®. The pristine film exhibited the characteristic absorption bands at wavenumbers of 1774 $cm^{-1}$, 1708 $cm^{-1}$, and 1367 $cm^{-1}$, which correspond to symmetric C=O, asymmetric C=O, and C-N-C vibration modes, respectively. The hydrolysis reaction by aqueous KOH led to imide-ring cleavage, thus resulting in significant reduction of the C=O imide absorption bands (1774 $cm^{-1}$ and 1708 $cm^{-1}$). There appeared new broad peaks at 1500 $cm^{-1}$ - 1700 $cm^{-1}$, which were superposition of carboxyl groups complexed with $K^+$ (1500 $cm^{-1}$ - 1600 $cm^{-1}$), C=O amide (1642 $cm^{-1}$), and N-H amide (1550 $cm^{-1}$) modes of the resulting polyamic metal salt.[42-44] A prolonged alkali hydroxylation reaction (> 15 min), however, led to degradation of the substrates, thereby compromising their physical properties.[45]

Immersion of the KOH-treated films in an aqueous $Zn^{2+}$ solution resulted in ion-exchange between $K^+$ and $Zn^{2+}$ as well as diffusion of $Zn^{2+}$ into the hydrophilic free volume. Although the ATR-FTIR spectra of both KOH-treated and $Zn^{2+}$ ion-exchanged film (hereafter, KAP-x-Zn for x min in KOH) were mostly indistinguishable, a decrease in absorption intensity of the spectra and formation of complex features in the region between 1500 $cm^{-1}$ - 1600 $cm^{-1}$ suggest the existence of several coordination states around the $Zn^{2+}$ complexes. The KAP-x-Zn was then solvothermally treated in a HmIm linker solution to form continuous ZIF-8 layers (hereafter, KAP-x-Zn-ZIF-8). As shown in the ATR-FTIR spectra, two new bands at 1145 $cm^{-1}$ (Fig. 2a) and 421 $cm^{-1}$ (Fig. S2b) appear, that can be assigned to the C-N and Zn-N bands of ZIF-8. The formation ZIF-8 crystal layers on the polymer substrates were also confirmed by powder X-ray diffraction (PXRD) patterns. All samples exhibit superimposed diffraction patterns of ZIF-8 and pristine Kapton® film. Interestingly, the intensities of the characteristic ZIF-8 peaks increase with hydrolysis time (Fig. 2b). The samples exhibit relatively similar degree of peak broadening, indicating the formation of ZIF-8 nanoparticles regardless of hydrolysis time. A plot of the relative (110) intensity provides a preliminary mean to estimate the relative increment in the amount of ZIF-8 nanocrystals formed as hydrolysis time increases. Since the concentration of $Zn^{2+}$ in the polymer is relatively low as compared to that of the linker, the number of ZIF-8 nanocrystals formed is expected to be limited by $Zn^{2+}$ concentration. The relative intensities of the (110) reflection are, therefore, directly related to the relative increment in $Zn^{2+}$ content in the modified polymer layer with respect to KOH treatment time. As shown in Fig. S4, the relative (110) intensity increases linearly with the degree of KOH hydrolysis, suggesting a systematic increment in the $Zn^{2+}$ content in the polymer substrates. This result agrees well with those previously reported.[36, 41, 43] Extending the hydrolysis reaction increases the number of $K^+$ in the modified layer. During ion-exchange process, the monovalent $K^+$ cations were replaced with divalent $Zn^{2+}$ cations. Also, the presence of more carboxylates due to the longer KOH treatment enhances the hydrophilicity of the substrates, which facilitates the mobility and the amount of free $Zn^{2+}$ ions into the polymer free volume. It is also worth mentioning here that films not subjected to the KOH treatment did not result in ZIF-8 crystals (Fig. S5). This highlights the importance of imide-ring opening through the hydrolysis reaction and subsequent ion-exchange with $Zn^{2+}$ for the nucleation and growth of ZIF-8 crystals.

To identify $Zn^{2+}$ bonding environment present in the polymer modified layer, X-ray photoelectron spectroscopy

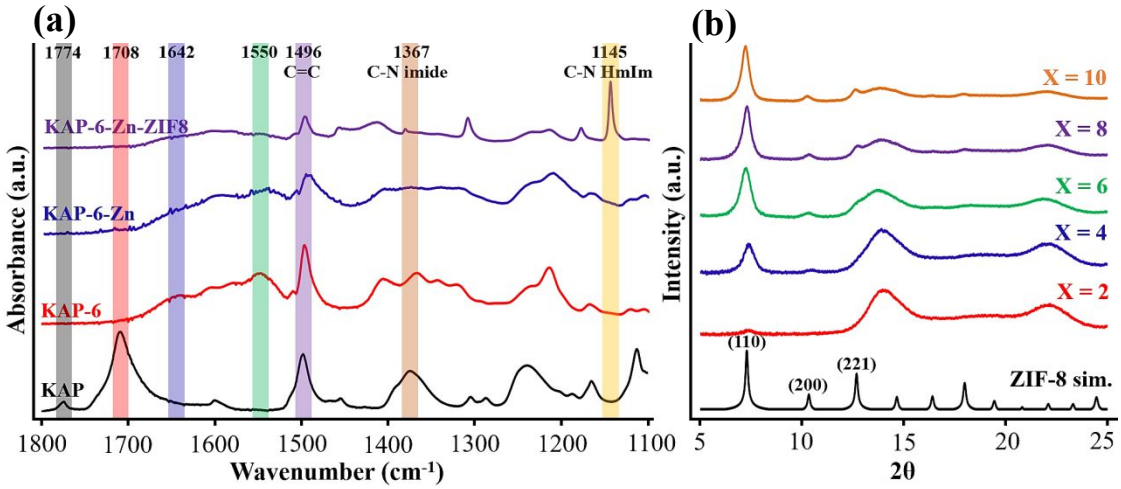


**Fig. 2.** (a) ATR-FTIR spectra of a pristine Kapton® film (KAP), hydrolyzed film for 6 min (KAP-6), $Zn^{2+}$-exchanged film (KAP-6-Zn), and ZIF-8 thin films synthesized using 6 min KOH treated film (KAP-6-Zn-ZIF-8) (b) PXRD patterns of ZIF-8 films synthesized over different KOH treatment time (KAP-x-Zn-ZIF-8 where x represents KOH treatment time in minutes) in comparison with the simulated one

(XPS) was performed on the $Zn^{2+}$-doped films. Fig. 3a shows the XPS spectra of the Zn $2p_{3/2}$ core level of the $Zn^{2+}$-doped films. The deconvolution of the Zn $2p_{3/2}$ core level gives out two separate peaks at 1022.5 eV and 1023.1 eV that can be assigned to Zn-polymer (i.e., coordinated ions) and Zn-water (i.e., free ions) interaction, respectively.[46, 47] Control experiments were performed to gain insight into which of these $Zn^{2+}$ ions (coordinated $Zn^{2+}$ vs. free $Zn^{2+}$) are most likely to participate in the ZIF-8 formation. A $Zn^{2+}$-doped film was washed with copious amount of DI water sufficiently long to remove free $Zn^{2+}$ ions in the free volume, leaving only the coordinated $Zn^{2+}$ ions in the polymer modified layer. Elution of free $Zn^{2+}$ ions from the film was monitored by periodically measuring the electrical conductivity of the DI water during the washing process. The washing step was terminated once the electrical conductivity of the DI water reaches steady-states (Fig. S6a). At this point, the elution of free $Zn^{2+}$ from the hydrophilic free volume was assumed to have completed and most of the free $Zn^{2+}$ have been removed. As shown Fig. S6b, a significant reduction in XPS peak intensity at a binding energy of 1023.1 eV suggests that most of the free $Zn^{2+}$ ions bound to water have been successfully removed. To our surprise, however, we observed a new peak at 1021 eV binding energy, assigned to another free $Zn^{2+}$. We believe the formation of this new peak may originate from the remaining free $Zn^{2+}$ present in the free volume in new binding environments due to longer contact in DI water. Nevertheless, the ratio between free and coordinated $Zn^{2+}$ has been decreased from 3.0 (rapid washing) to 1.4 (extensive washing). After solvothermal reaction in a HmIm solution, the $Zn^{2+}$-doped film subjected to extensive washing shows a significantly weaker ZIF-8 diffraction peak as compared to that after quick washing as shown in Fig. S7. This observation strongly suggests that the $Zn^{2+}$ ions coordinating with carboxylic groups do not participate in the formation of ZIF-8 crystals. This is attributed to the fact that the coordinated $Zn^{2+}$ ions cannot be easily liberated possibly due to the relatively low concentration of counter cations (i.e., $H^+$) present in the linker solution (pH ~ 9.9) and the use of relatively mild reaction temperature (120 °C).[36, 48] It is noted that Tsuruoka et al.[36] used microwave heating where the strong interaction between microwaves and coordinated cations in the polymer led to a rapid increase in the local temperature, thereby liberating coordinated $Al^{3+}$ ions.

Scanning electron microscopy (SEM) images in Fig. 3(b - f) and optical images in Fig. S8 display the temporal evolution of KAP-x-Zn-ZIF-8 as a function of KOH treatment time. With an exception of KAP-2-Zn-ZIF-8, the samples formed continuous ZIF-8 crystal layers on top, implying that there exists a minimum amount of metal-ion dopants required to form continuous ZIF-8 films on the substrate surface. The crystallite sizes were determined approximately 40.3 ± 7.6 nm, which is comparable with the crystallite sizes calculated using the Scherer equation (33.7 ± 7.0 nm). Cross-sectional SEM images, however, revealed a very interesting morphology which has never been previously observed. As shown in the inset cross-sectional images, ZIF-8 crystals appeared to be embedded (shown in yellow circles) and uniformly distributed in the polymer matrix and this composite layer thickness increased linearly with KOH treatment time (Fig. S9). The linear depth modification profile observed in this study is consistent with the previous observations by Stoffel et al.[49] and Lee et al.[50] As mentioned by Stoffel and co-workers,[49] the growth rate of the KOH-modified layer was governed by the kinetics of hydrolysis of the imide rings at the modified and unmodified layer interface. In their study,[49] they found that the kinetics of hydrolysis at the interface were constant regardless of modification depth. Constant hydrolysis kinetics led to constant growth kinetics, and this result in a linear depth

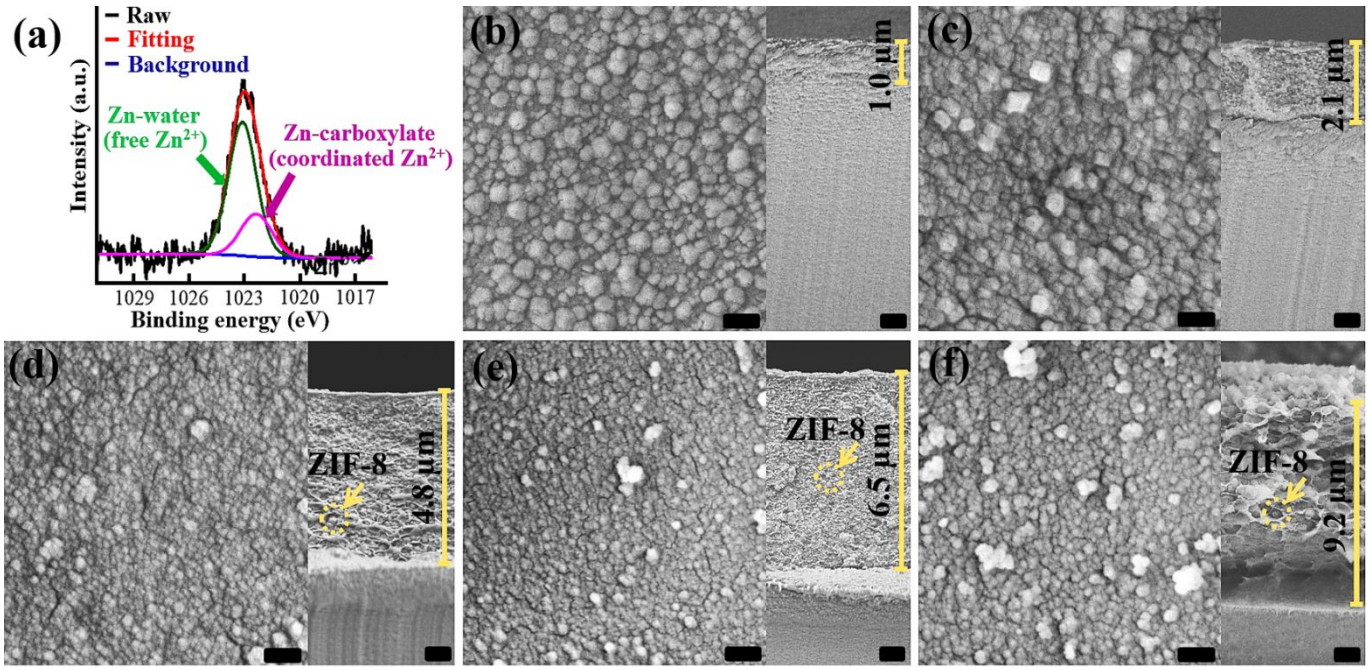


**Fig. 3.** (a) High resolution XPS spectra of the $Zn^{2+}$-exchanged Kapton® film. Top and cross-sectional SEM images of the films synthesized using polymer substrates immersed in KOH for (b) 2 min, (c) 4 min, (d) 6 min, (e) 8 min, and (f) 10 min. Top image scale bar: 200 nm. Inset cross section image scale bar: 1 μm

modification profile of the polymer as a function of KOH treatment time.

To confirm the formation of ZIF-8 crystals inside the polymers, a quick acid treatment was performed to remove surface-bound crystals from the samples. KAP-6-Zn-ZIF-8 samples were subjected to a diluted acid wipe (0.05 M $HNO_3$) for several cycles and PXRD patterns were collected after each cycle. A plot of the relative (110) intensity with the number of acid treatment cycles was constructed, serving as an indirect indicator of the relative amount of ZIF-8 formed inside vs. outside the polymer (Fig. S10). After five acid treatment cycles, the relative (110) intensity remains almost constant (~ 60 %). After initial removal of the surface-bound crystals, further removal of ZIF-8 by dilute $HNO_3$ are thwarted as the remaining ZIF-8 crystals are embedded and protected in the polymer matrix. Top SEM images and energy dispersive X-ray (EDX) line scan analysis performed on the surface of the acid treated samples confirmed a complete removal of the surface-bound ZIF-8 crystals. On the other hand, cross-sectional SEM images revealed that most of the ZIF-8 crystals formed inside the polymer remained intact even after subjected to eight acid treatment cycles (Fig. S11). As opposed to KAP-6-Zn-ZIF-8, the relative (110) intensity of KAP-2-Zn-ZIF-8 was reduced to 0 % after subjected to similar acid treatment cycles as shown in Fig. S10b, suggesting ZIF-8 crystals formed mostly on the polymer surface. This strongly indicates that one can control the location of ZIF-8 crystals by simply adjusting the hydrolysis time.

Fig. 4 presents microstructure of a representative KAP-6-Zn-ZIF-8 sample, showing that the size of the embedded ZIF-8 particles detected under SEM (Fig. 4b) and TEM (Fig. 4c) was comparable. Although the observed particle shown in Fig. 4c appears to be a ZIF-8 single crystal, the inset electron diffraction suggests that the particle consist of several smaller ZIF-8 crystals but of unknown sizes (see also Fig. S12a). TEM analysis also revealed the formation of some unknown amorphous phases inside the polymer (Fig. S12b). To the best of our knowledge, *in-situ* formation of ZIF-8 inside the polymer has never been reported previously. It is surmised that during the solvothermal reaction in a linker solution, ZIF-8 crystals formed not only at the polymer/solution interface[36] but also inside the polymer possibly due to the slow elution of free $Zn^{2+}$ ions from the polymer free volume, thereby allowing linker molecules to diffuse deep into and consequently crystallizing inside the modified layer. Inside the free volume spaces, several nuclei might form, resulting in ZIF-8 particles of several grains inside the polymer. It is worthy of noting that the ability to *in-situ* form ZIF-8 nanoparticles inside polymer substrates bears a significant implication for the one-step synthesis of ZIF-8/polymer composite films and membranes.

In addition to ZIF-8, the PMMOF process was also applied to synthesize thin films of ZIF-67 (Co-substituted ZIF-8) and Zn/Co mixed-metal ZIFs (hereafter, $Zn_xCo_{1-x}$-ZIF-8). A great deal of research has been undertaken to fine tune the properties (e.g., pore aperture, pore volume, functionality, etc.) of MOFs by mixed-metal[51, 52] and mixed-linker[53, 54] approaches. Versatility of the PMMOF process not only allows one to use different metal dopants (i.e., $Co^{2+}$) but also to tailor the composition of co-dopants (i.e., $Zn^{2+}$ and $Co^{2+}$) in the polymer modified layer, thereby enabling construction of monometallic and bi-metallic ZIF films with rational control over metal compositions in the frameworks. ZIF-67 films were readily prepared by simply replacing the metal dopant from $Zn^{2+}$ to $Co^{2+}$. On the other hand, $Zn_xCo_{1-x}$-ZIF-8 films were synthesized by doping the polymer substrates with a mixture of metal cations (i.e., $Zn^{2+}$ and $Co^{2+}$) of known composition. As a proof-of-concept, an aqueous mixture of zinc nitrate hexahydrate (50 mM) and cobalt nitrate hexahydrate (50 mM) was used during ion-exchange, forming an equimolar mixture of the dopant species in the ZIF frameworks ($Zn_{0.5}Co_{0.5}$-ZIF-8). All samples were subjected to similar KOH treatment time of 6 min (KAP-6) and the subsequent reaction conditions were maintained the same.

The PXRD patterns in Fig. S13 confirmed the formation of phase-pure ZIF-8, $Zn_{0.5}Co_{0.5}$-ZIF-8, and ZIF-67 crystals. The resulting ZIF thin films are presented in Fig. 5 where several observations can be made. First, ZIF-8, $Zn_{0.5}Co_{0.5}$-ZIF-8, and ZIF-67 crystals were densely-packed, yielding continuous films on the substrates. Second, the films were made of grains with a relatively narrow size distribution and the sizes of these grains appeared to be systematically increasing in the following order, ZIF-8 < $Zn_{0.5}Co_{0.5}$-ZIF-8 < ZIF-67 (40 nm vs. 155 nm vs. 271 nm). The difference in the crystallite sizes can be attributed to slower nucleation and different crystal-growth kinetics upon incorporation of $Co^{2+}$ in the $Zn^{2+}$-doped substrates.[52] For Zn/Co mixed-metal ZIF, interestingly, incorporation of $Co^{2+}$ and $Zn^{2+}$ into the framework can be monitored through direct optical observation of color change. To further confirm the

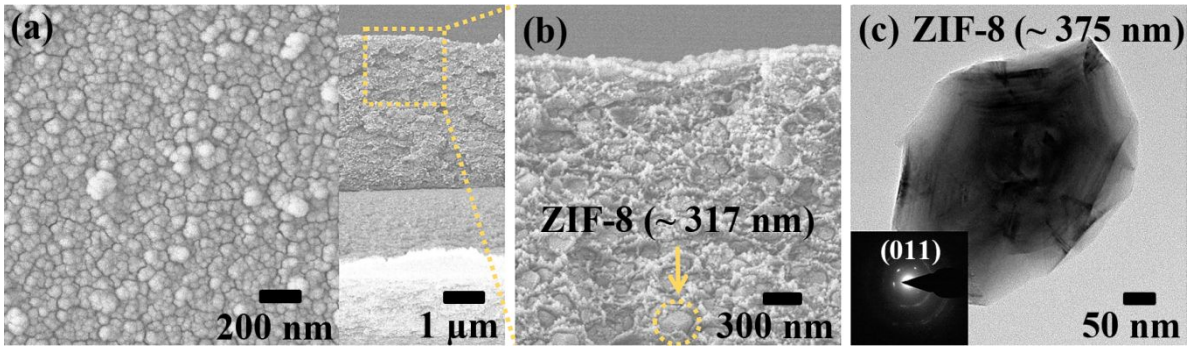


**Fig. 4.** (a) Top and cross-sectional SEM images of KAP-6-Zn-ZIF-8, (b) magnified view of the selected area in (a), and (c) cross-sectional TEM image of ZIF-8 crystals with electron diffraction pattern (inset)

incorporation of $Zn^{2+}$ and $Co^{2+}$ in ZIF frameworks, EDX line profile analysis was performed. The EDX line scan analysis of $Zn_{0.5}Co_{0.5}$-ZIF-8 surfaces in Fig. 5b shows that $Zn^{2+}$ and $Co^{2+}$ were uniformly distributed throughout the surface. The relative amount between $Zn^{2+}$ and $Co^{2+}$ was close to unity and was found to be consistent with those of co-doped polymer substrates (Fig. S14 and S15).

Additionally, metal-to-nitrogen absorption bands of $Zn_{0.5}Co_{0.5}$-ZIF-8 became broader and blue-shifted upon incorporation of $Co^{2+}$ into the ZIF-8 frameworks, which agrees with the previous report.[55] $Zn_{0.5}Co_{0.5}$-ZIF-8 (Zn/Co mixed-metal ZIF) consisting of more rigid Co-N (i.e., stiffer) and less rigid Zn-N bonds alter metal-to-nitrogen stretching frequency, thus leading to the blue-shift.[17] An ability to control dopants and their compositions in polymer substrates present an unprecedented opportunity to fabricate important monometallic family of ZIFs and bimetallic ZIF films for a variety of applications. Finally, site-selective interfacial reaction allows for construction of one and/or multiple types of ZIF films grown on specific locations on polymer substrates.[56] When ion-exchanged with $Co^{2+}$ on one side and $Zn^{2+}$ on the other side (Fig. S16), ZIF-67 and ZIF-8 films were formed on different sides (i.e., Janus MOF films).

Based on the proposed mechanism illustrated in Fig. 1, it is postulated that the PMMOF process can be readily extended to fabricate ZIF-8 thin films on different polymer-based substrates with various geometries, provided that the substrates are able to undergone similar chemistry. To test our hypothesis, we attempted to fabricate ZIF-8 thin films on porous Matrimid® flat sheet and hollow fibers (Fig. S17 and S18). Matrimid® flat sheets were prepared by the dry-wet phase inversion method while Matrimid® hollow fibers were fabricated by a dry-wet jet spinning process. The pristine hollow fibers were macroporous ($N_2$ permeance ~ 45,594 GPU, 1 gas permeation unit (GPU) = $3.348 \times 10^{-10}$ mol $m^{-2}$ $s^{-1}$ $Pa^{-1}$) with inner and outer diameter of 465 µm and 590 µm, respectively. As can be seen in Fig. S17, thin polycrystalline ZIF-8 layers were successfully grown on Matrimid® flat sheets using the PMMOF process. Similarly, in Fig. 6(b - inset), densely-packed-nanometer-sized ZIF-8 crystal layers with a uniform surface coverage were successfully deposited on the bore side of the hollow fibers using the similar approach. This finding is of particular importance as the proposed approach can provide a new means to synthesize well-intergrown films and/or membranes on commercially available polyimide-based hollow fibers especially for separation applications.

The ZIF-8 seed crystals on Matrimid® hollow fibers obtained using the PMMOF processes were secondarily grown into ZIF-8 membranes under a continuous microfluidic flow of a growth solution. The resulting ZIF-8 membranes supported on Matrimid® hollow fibers were well-intergrown without any macroscopic defects, with thickness of ~ 900 nm. The propylene/propane separation performances of the membranes were tested using the Wicke-Kallenbach technique conducted at room temperature. The ZIF-8 membrane module used for propylene/propane permeation test has an active membrane area of 0.584 $cm^2$. An equimolar (50:50) propylene/propane gas mixture was fed to the feed (bore) side

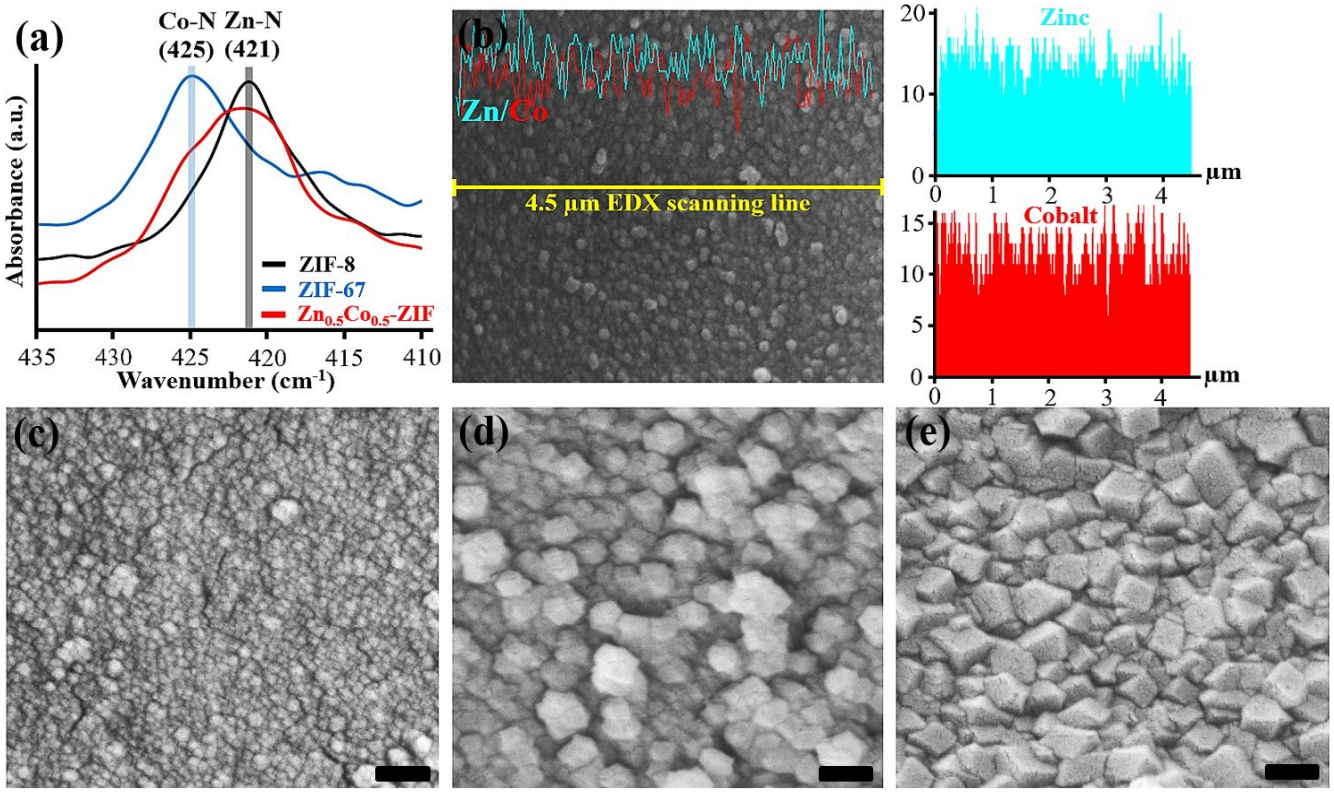


**Fig. 5.** (a) ATR-FTIR spectra showing metal-to-nitrogen stretching vibrations of different ZIF thin films and (b) EDX line scan analysis on $Zn_{0.5}Co_{0.5}$-ZIF-8 film surface. Top SEM images of (c) ZIF-8, (d) $Zn_{0.5}Co_{0.5}$-ZIF-8, and (e) ZIF-67 thin film on polymer substrates. Top view scale bar: 200 nm

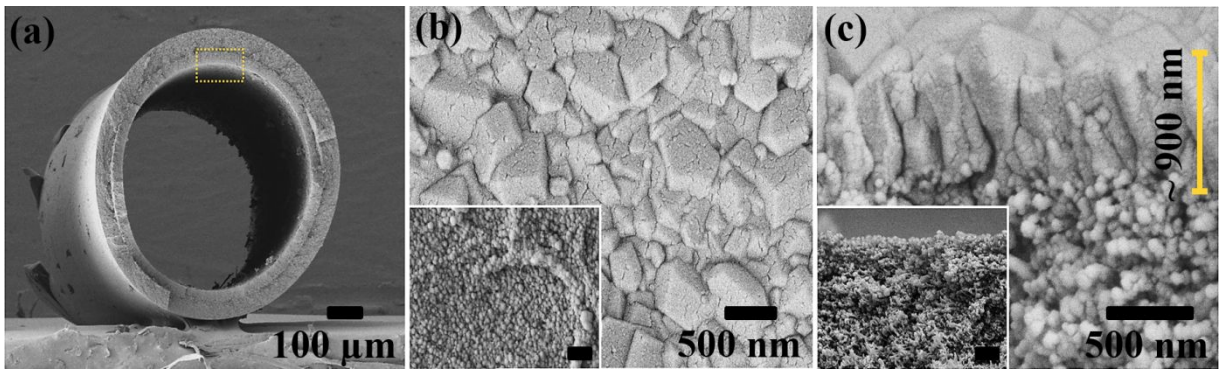


**Fig. 6.** (a) Cross section view of ZIF-8 membranes under low magnification (b) top and (c) cross section view of the ZIF-8 membrane and seed crystals (inset) in higher magnification. Inset image scale bar: 500 nm

while argon sweep gas was provided to permeate (shell) side. Volumetric flow rates of both feed and sweep gases were set at 20 cc/min. The as-prepared ZIF-8 membranes on Matrimid® hollow fibers unfortunately did not display good propylene/propane separation performances presumably due to relatively poor grain boundary defects. A thin polydimethylsiloxane coating[57] was applied on top of the membranes to seal those defects and the resulting ZIF-8 membranes showed much improved separation performances. The average propylene permeances and propylene/propane separation factor of the supported ZIF-8 membranes were ~ 195 $\times$ $10^{-10}$ mol $m^{-2}$ $s^{-1}$ $Pa^{-1}$ (~ 59 GPU) and 27, respectively, which are somewhat promising. The separation performances of our ZIF-8 membranes on Matrimid® hollow fibers were compared to those reported in literature and the comparison includes the ZIF-8 membranes grown on flat disc (inorganic and organic substrates). As shown in Fig. S19, the propylene permeability of our ZIF-8 membranes were comparable to those reported (permeability ~ 54.2 Barrer). However, the propylene/propane separation factor of our ZIF-8 membranes (separation factor ~ 27) need to be further improved to a minimum separation factor of 35 required to be considered 'commercially attractive'. Optimization of ZIF-8 seeding and secondary growth steps are currently underway to improve microstructure of the ZIF-8 membranes on Matrimid® hollow fibers. Our finding regarding the optimized ZIF-8 membrane formation on Matrimid® hollow fibers including their improved gas separation performances will be discussed in detail in a forthcoming report.

## Conclusions

In conclusion, we have developed and demonstrated a simple methodology (termed as PMMOF) for facile synthesis of ZIF-8 thin films on polymer substrates and ZIF-8/polymer composites using ion-exchanged polymer substrates followed by conventional solvothermal reaction. While continuous and densely-packed ZIF-8 crystal layers were observed on the polymer surfaces, ZIF-8/polymer mixed-matrix layers were also observed inside the polymer substrates. Adjusting hydrolysis time was found a simple means to control the location of ZIF-8 crystals forming. The PMMOF approach was applied to different ZIFs (i.e., ZIF-67) and/or mixed-metal ZIFs (i.e., ZnxCo1-x-ZIF-8) as well as to different polyimide-based substrates with different geometries, showing the versatility of the approach. Furthermore, the PMMOF approach utilizing interfacial reaction on metal-doped polymer substrates is found location-selective, potentially enabling the construction of complex patterns of MOFs. Finally, ultra-thin ZIF-8 membranes on porous Matrimid® hollow fibers were demonstrated by secondarily growing ZIF-8 seed crystal layers deposited on the bore sides of the hollow fibers by the PMMOF. The membranes exhibited promising propylene/propane separation performances once coated with PDMS. It is expected that the PMMOF approach reported here can potentially open up new possibilities to readily fabricate MOF crystals on and inside polymer substrates for a variety of advanced applications including gas separation, catalysis, and sensing.

## Conflicts of interest

There are no conflicts to declare.

## Acknowledgements

H.-K.J. acknowledges the financial support from the National Science Foundation (CBET-1510530). This publication was made possible in part by NPRP grant # 8-001-2-001 from the Qatar National Research Fund (a member of Qatar Foundation). The findings achieved herein are solely the responsibility of the authors. The National Science Foundation supported the FE-SEM acquisition under Grant DBI-0116835, the VP for Research Office, and the Texas A&M Engineering Experimental Station.

## References

1. L. J. Murray, M. Dincă and J. R. Long, *Chem. Soc. Rev.*, 2009, **38**, 1294-1314.
2. J.-R. Li, J. Sculley and H.-C. Zhou, *Chem. Rev.*, 2011, **112**, 869-932.
3. L. E. Kreno, K. Leong, O. K. Farha, M. Allendorf, R. P. Van Duyne and J. T. Hupp, *Chem. Rev.*, 2011, **112**, 1105-1125.
4. J. Lee, O. K. Farha, J. Roberts, K. A. Scheidt, S. T. Nguyen and J. T. Hupp, *Chem. Soc. Rev.*, 2009, **38**, 1450-1459.
5. B. Wang, A. P. Côté, H. Furukawa, M. O'Keeffe and O. M. Yaghi, *Nature*, 2008, **453**, 207.

6. K. S. Park, Z. Ni, A. P. Côté, J. Y. Choi, R. Huang, F. J. Uribe-Romo, H. K. Chae, M. O'Keeffe and O. M. Yaghi, *Proc. Natl. Acad. Sci. U.S.A.*, 2006, **103**, 10186-10191.
7. A. U. Czaja, N. Trukhan and U. Müller, *Chem. Soc. Rev.*, 2009, **38**, 1284-1293.
8. P. Silva, S. M. Vilela, J. P. Tomé and F. A. A. Paz, *Chem. Soc. Rev.*, 2015, **44**, 6774-6803.
9. O. Shekhah, J. Liu, R. Fischer and C. Wöll, *Chem. Soc. Rev.*, 2011, **40**, 1081-1106.
10. J. Liu and C. Wöll, *Chem. Soc. Rev.*, 2017, **46**, 5730-5770.
11. T.-S. Chung, L. Y. Jiang, Y. Li and S. Kulprathipanja, *Prog. Polym. Sci.*, 2007, **32**, 483-507.
12. G. Dong, H. Li and V. Chen, *J. Mater. Chem. A*, 2013, **1**, 4610-4630.
13. M. R. A. Hamid and H.-K. Jeong, *Korean J. Chem. Eng.*, 2018, **35**, 1577-1600.
14. Y. Pan, T. Li, G. Lestari and Z. Lai, *J. Membr. Sci.*, 2012, **390**, 93-98.
15. M. Shah, H. T. Kwon, V. Tran, S. Sachdeva and H.-K. Jeong, *Microporous Mesoporous Mater.*, 2013, **165**, 63-69.
16. H. T. Kwon and H.-K. Jeong, *J. Am. Chem. Soc.*, 2013, **135**, 10763-10768.
17. H. T. Kwon, H.-K. Jeong, A. S. Lee, H. S. An and J. S. Lee, *J. Am. Chem. Soc.*, 2015, **137**, 12304-12311.
18. E. Shamsaei, X. Lin, Z.-X. Low, Z. Abbasi, Y. Hu, J. Z. Liu and H. Wang, *ACS Appl. Mater. Interfaces*, 2016, **8**, 6236-6244.
19. F. Cacho-Bailo, B. Seoane, C. Téllez and J. Coronas, *J. Membr. Sci.*, 2014, **464**, 119-126.
20. W. Li, Z. Yang, G. Zhang, Z. Fan, Q. Meng, C. Shen and C. Gao, *J. Mater. Chem. A*, 2014, **2**, 2110-2118.
21. A. J. Brown, J. Johnson, M. E. Lydon, W. J. Koros, C. W. Jones and S. Nair, *Angew. Chem.*, 2012, **51**, 10615-10618.
22. L. Ge, W. Zhou, A. Du and Z. Zhu, *J. Phys. Chem. C*, 2012, **116**, 13264-13270.
23. E. Barankova, N. Pradeep and K.-V. Peinemann, *Chem. Commun.*, 2013, **49**, 9419-9421.
24. P. Neelakanda, E. Barankova and K.-V. Peinemann, *Microporous Mesoporous Mater.*, 2016, **220**, 215-219.
25. M. Meilikhov, K. Yusenko, E. Schollmeyer, C. Mayer, H.-J. Buschmann and R. A. Fischer, *Dalton Trans.*, 2011, **40**, 4838-4841.
26. K. Eum, C. Ma, A. Rownaghi, C. W. Jones and S. Nair, *ACS Appl. Mater. Interfaces*, 2016, **8**, 25337-25342.
27. Y. Li, L. H. Wee, A. Volodin, J. A. Martens and I. F. Vankelecom, *Chem. Commun.*, 2015, **51**, 918-920.
28. A. Centrone, Y. Yang, S. Speakman, L. Bromberg, G. C. Rutledge and T. A. Hatton, *J. Am. Chem. Soc.*, 2010, **132**, 15687-15691.
29. J. Yao, D. Dong, D. Li, L. He, G. Xu and H. Wang, *Chem. Commun.*, 2011, **47**, 2559-2561.
30. D. Nagaraju, D. G. Bhagat, R. Banerjee and U. K. Kharul, *J. Mater. Chem. A*, 2013, **1**, 8828-8835.
31. A. J. Brown, N. A. Brunelli, K. Eum, F. Rashidi, J. Johnson, W. J. Koros, C. W. Jones and S. Nair, *Science*, 2014, **345**, 72-75.
32. J. Hou, P. D. Sutrisna, Y. Zhang and V. Chen, *Angew. Chem.*, 2016, **55**, 3947-3951.
33. W. Li, P. Su, Z. Li, Z. Xu, F. Wang, H. Ou, J. Zhang, G. Zhang and E. Zeng, *Nat. Commun.*, 2017, **8**, 406.
34. F. Cacho-Bailo, S. Catalan-Aguirre, M. Etxeberria-Benavides, O. Karvan, V. Sebastian, C. Tellez and J. Coronas, *J. Membr. Sci.*, 2015, **476**, 277-285.
35. M. J. Lee, M. R. A. Hamid, J. Lee, J. S. Kim, Y. M. Lee and H.-K. Jeong, *J. Membr. Sci.*, 2018.
36. T. Tsuruoka, M. Kumano, K. Mantani, T. Matsuyama, A. Miyanaga, T. Ohhashi, Y. Takashima, H. Minami, T. Suzuki and K. Imagawa, *Cryst. Growth Des.*, 2016, **16**, 2472-2476.
37. T. Tsuruoka, K. Mantani, A. Miyanaga, T. Matsuyama, T. Ohhashi, Y. Takashima and K. Akamatsu, *Langmuir*, 2016, **32**, 6068-6073.
38. T. Ohhashi, T. Tsuruoka, S. Fujimoto, Y. Takashima and K. Akamatsu, *Cryst. Growth Des.*, 2017, **18**, 402-408.
39. K. T. Woo, J. Lee, G. Dong, J. S. Kim, Y. S. Do, H. J. Jo and Y. M. Lee, *J. Membr. Sci.*, 2016, **498**, 125-134.
40. J. Mulder, *Basic principles of membrane technology*, Springer Science & Business Media, 2012.
41. S. Yang, D. Wu, S. Qi, G. Cui, R. Jin and Z. Wu, *J. Phys. Chem. B*, 2009, **113**, 9694-9701.
42. S. Ikeda, K. Akamatsu, H. Nawafune, T. Nishino and S. Deki, *J. Phys. Chem. B*, 2004, **108**, 15599-15607.
43. K. Akamatsu, S. Ikeda, H. Nawafune and S. Deki, *Chem. Mater.*, 2003, **15**, 2488-2491.
44. S. Mu, Z. Wu, Y. Wang, S. Qi, X. Yang and D. Wu, *Thin Solid Films*, 2010, **518**, 4175-4182.
45. X. D. Huang, S. M. Bhangale, P. M. Moran, N. L. Yakovlev and J. Pan, *Polym. Int.*, 2003, **52**, 1064-1069.
46. M. Wang, L. Jiang, E. J. Kim and S. H. Hahn, *RSC Adv.*, 2015, **5**, 87496-87503.
47. D. Pradhan, S. Sindhwani and K. Leung, *J. Phys. Chem. C*, 2009, **113**, 15788-15791.
48. S. Mu, D. Wu, S. Qi and Z. Wu, *J. Nanomater.*, 2011, **2011**, 38.
49. N. C. Stoffel, M. Hsieh, S. Chandra and E. Kramer, *Chem. Mater.*, 1996, **8**, 1035-1041.
50. K. W. Lee, S. P. Kowalczyk and J. M. Shaw, *Macromolecules*, 1990, **23**, 2097-2100.
51. T. Tsuruoka, A. Miyanaga, T. Ohhashi, M. Hata, Y. Takashima and K. Akamatsu, *J. Solid State Chem.*, 2017, **253**, 43-46.
52. C. Wang, F. Yang, L. Sheng, J. Yu, K. Yao, L. Zhang and Y. Pan, *Chem. Commun.*, 2016, **52**, 12578-12581.
53. K. Eum, K. C. Jayachandrababu, F. Rashidi, K. Zhang, J. Leisen, S. Graham, R. P. Lively, R. R. Chance, D. S. Sholl and C. W. Jones, *J. Am. Chem. Soc.*, 2015, **137**, 4191-4197.
54. L. Huang, M. Xue, Q. Song, S. Chen, Y. Pan and S. Qiu, *Inorg. Chem. Commun.*, 2014, **46**, 9-12.
55. F. Hillman, J. M. Zimmerman, S.-M. Paek, M. R. Hamid, W. T. Lim and H.-K. Jeong, *J. Mater. Chem. A*, 2017, **5**, 6090-6099.
56. T. Tsuruoka, T. Matsuyama, A. Miyanaga, T. Ohhashi, Y. Takashima and K. Akamatsu, *RSC Adv.*, 2016, **6**, 77297-77300.
57. L. Sheng, C. Wang, F. Yang, L. Xiang, X. Huang, J. Yu, L. Zhang, Y. Pan and Y. J. C. C. Li, *Chem. Commun.*, 2017, **53**, 7760-7763.

# *In-Situ* Formation of Zeolitic-Imidazolate Framework Thin Films and Composites Using Modified Polymer Substrates

Mohamad Rezi Abdul Hamid, Sunghwan Park, Ju Sung Kim, Young Moo Lee and Hae-Kwon Jeong*

* Corresponding author: hjeong7@tamu.edu

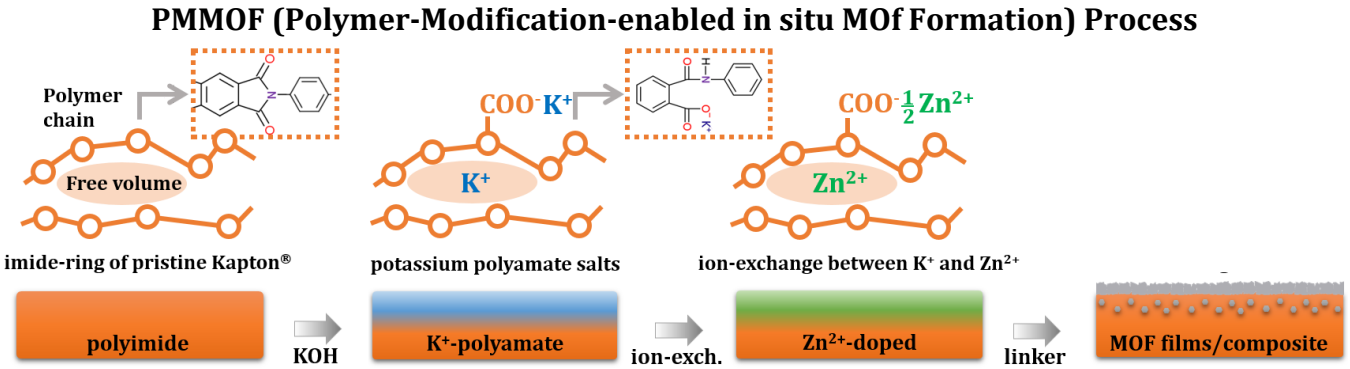


*In-situ* formation of multifunctional MOF thin films and composites using the PMMOF process